

ARTICLE

Received 7 Aug 2014 | Accepted 10 Sep 2014 | Published 15 Oct 2014

DOI: 10.1038/ncomms6245

OPEN

# Increasing microtubule acetylation rescues axonal transport and locomotor deficits caused by LRRK2 Roc-COR domain mutations

Vinay K. Godena<sup>1,2,3,\*</sup>, Nicholas Brookes-Hocking<sup>4,\*</sup>, Annkathrin Moller<sup>5</sup>, Gary Shaw<sup>5</sup>, Matthew Oswald<sup>1,2,†</sup>, Rosa M. Sancho<sup>4,†</sup>, Christopher C.J. Miller<sup>4</sup>, Alexander J. Whitworth<sup>1,2,3</sup> & Kurt J. De Vos<sup>3,5</sup>

*Leucine-rich repeat kinase 2 (LRRK2)* mutations are the most common genetic cause of Parkinson's disease. LRRK2 is a multifunctional protein affecting many cellular processes and has been described to bind microtubules. Defective microtubule-based axonal transport is hypothesized to contribute to Parkinson's disease, but whether LRRK2 mutations affect this process to mediate pathogenesis is not known. Here we find that LRRK2 containing pathogenic Roc-COR domain mutations (R1441C, Y1699C) preferentially associates with deacetylated microtubules, and inhibits axonal transport in primary neurons and in *Drosophila*, causing locomotor deficits *in vivo*. *In vitro*, increasing microtubule acetylation using deacetylase inhibitors or the tubulin acetylase  $\alpha$ TAT1 prevents association of mutant LRRK2 with microtubules, and the deacetylase inhibitor trichostatin A (TSA) restores axonal transport. *In vivo* knockdown of the deacetylases HDAC6 and Sirt2, or administration of TSA rescues both axonal transport and locomotor behavior. Thus, this study reveals a pathogenic mechanism and a potential intervention for Parkinson's disease.

<sup>1</sup>Department of Biomedical Sciences, University of Sheffield, Firth Court, Western Bank, Sheffield S10 2TN, UK. <sup>2</sup>The Bateson Centre, University of Sheffield, Sheffield S10 2TN, UK. <sup>3</sup>Centre for Membrane Interactions and Dynamics, University of Sheffield, Sheffield S10 2TN, UK. <sup>4</sup>Department of Basic and Clinical Neuroscience, Institute of Psychiatry, Psychology and Neuroscience, King's College London, De Crespigny Park, Denmark Hill, London SE5 8AF, UK.

<sup>5</sup>Department of Neuroscience, Sheffield Institute for Translational Neuroscience (SITraN), University of Sheffield, 385a Glossop Road, Sheffield S10 2HQ, UK.

\* These authors contributed equally to this work. † Present addresses: Department of Zoology, University of Cambridge, Downing Street, Cambridge CB2 3EJ, UK (M.O.); Alzheimer's Research UK, Unit 3 Riverside, Granta Park, Cambridge CB21 6AD, UK (R.M.S.). Correspondence and requests for materials should be addressed to A.J.W. (email: a.whitworth@sheffield.ac.uk) or to K.J.D.V. (email: k.de\_vos@sheffield.ac.uk).

**D**ominant mutations in *leucine-rich repeat kinase 2* (*LRRK2*) are the most common genetic cause of Parkinson's disease (PD), and genome-wide association studies have highlighted the *LRRK2* locus as a risk factor for sporadic PD<sup>1–5</sup>. *LRRK2* is a multifunctional, multi-domain protein and dominant mutations have been identified in the Ras of complex (Roc) GTPase protein domain (R1441C, R1441G, R1441H), the carboxy-terminal of Roc (COR) domain (Y1699C) and the kinase domain (G2019S and I2020T). Mutations in the Roc and COR domains decrease GTPase activity<sup>6,7</sup>, whereas the G2019S mutation increases kinase activity<sup>6,8,9</sup>. How *LRRK2* mutations confer toxicity is not yet clear, but may involve the possible physiological function of *LRRK2* in the maintenance of axonal integrity. Indeed, there is evidence that the overexpression of *LRRK2* causes neurite shortening, whereas the loss of *LRRK2* function in mouse neurons results in elongation of neuronal processes and increased branching<sup>10–13</sup>. The molecular details underlying mutant *LRRK2*'s effects on neurites are not fully understood, but may involve interactions with microtubules<sup>14–18</sup>. The architecture of neurons makes them particularly dependent on efficient intracellular transport of cargoes such as organelles and proteins to maintain structural integrity and function. Since defective axonal transport, which utilizes microtubules as transport tracks, has been proposed as a mechanism for PD<sup>19–24</sup>, we hypothesized that mutant *LRRK2* may disturb microtubule-based axonal transport.

Here we show that *LRRK2* Roc-COR mutants disrupt axonal transport *in vitro* and *in vivo* to induce locomotor deficits by binding to deacetylated microtubules. Increasing microtubule acetylation prevents microtubule association, restores axonal transport and rescues locomotor deficits caused by *LRRK2* Roc-COR mutants. Thus, our data reveals a pathogenic mechanism and a potential therapeutic intervention for PD.

## Results

### Roc-COR mutations inhibit axonal transport and locomotion.

To study the effect of pathogenic *LRRK2* mutations on axonal transport, we expressed wild-type (WT) or mutant (R1441C, Y1699C or G2019S) *LRRK2* variants in rat cortical neuron cultures, and analysed the movement of mitochondria from time-lapse recordings. Whereas the expression of *LRRK2*-WT or *LRRK2*-G2019S did not affect mitochondrial transport, both *LRRK2*-R1441C and *LRRK2*-Y1699C significantly inhibited the transport of mitochondria by disrupting both anterograde and retrograde motility (Fig. 1a). Detailed analysis revealed that both *LRRK2*-R1441C and *LRRK2*-Y1699C decreased anterograde and retrograde transport frequencies, with a concomitant increase in the duration of pauses and decreased velocities (Supplementary Fig. 1).

To investigate if this axonal transport defect occurred *in vivo*, we analysed the transport of mitochondria in motor neurons of *Drosophila* larvae expressing human *LRRK2* variants. Similar to mammalian neurons, the expression of *LRRK2*-WT or *LRRK2*-G2019S did not adversely affect mitochondrial transport, whereas the *LRRK2*-R1441C or *LRRK2*-Y1699C mutants reduced the number of motile mitochondria in both anterograde and retrograde directions (Fig. 1b). Moreover, the effects are evolutionarily conserved as the expression of *Drosophila* *Lrrk*-R1069C (equivalent to *LRRK2*-R1441C) or *Lrrk*-Y1383C (equivalent to *LRRK2*-Y1699C) inhibited both anterograde and retrograde transport, while the expression of *Lrrk*-WT similarly had no effect on transport (Supplementary Fig. 2). Together these results demonstrate that the expression of pathogenic Roc-COR variants of *LRRK2* or its *Drosophila* homologue *Lrrk* inhibit bidirectional axonal transport of mitochondria *in vitro* and *in vivo*.

The *Drosophila* model enabled us to investigate whether the aberrant axonal transport resulted in a functional deficit of the motor system. Adult flies expressing variant forms of *LRRK2* or *Lrrk* in motor neurons were assayed for climbing and flight ability. Flies expressing WT *LRRK2*/*Lrrk* or *LRRK2*-G2019S showed no defect in locomotion compared with controls, consistent with a lack of effect on axonal transport (Fig. 1c and Supplementary Fig. 2). However, *LRRK2*-R1441C and *LRRK2*-Y1699C caused a significant decrease in both climbing and flight ability (Fig. 1c). Consistent with a conserved effect of these mutations, *Lrrk*-R1069C and *Lrrk*-Y1383C also caused locomotor deficits (Supplementary Fig. 2).

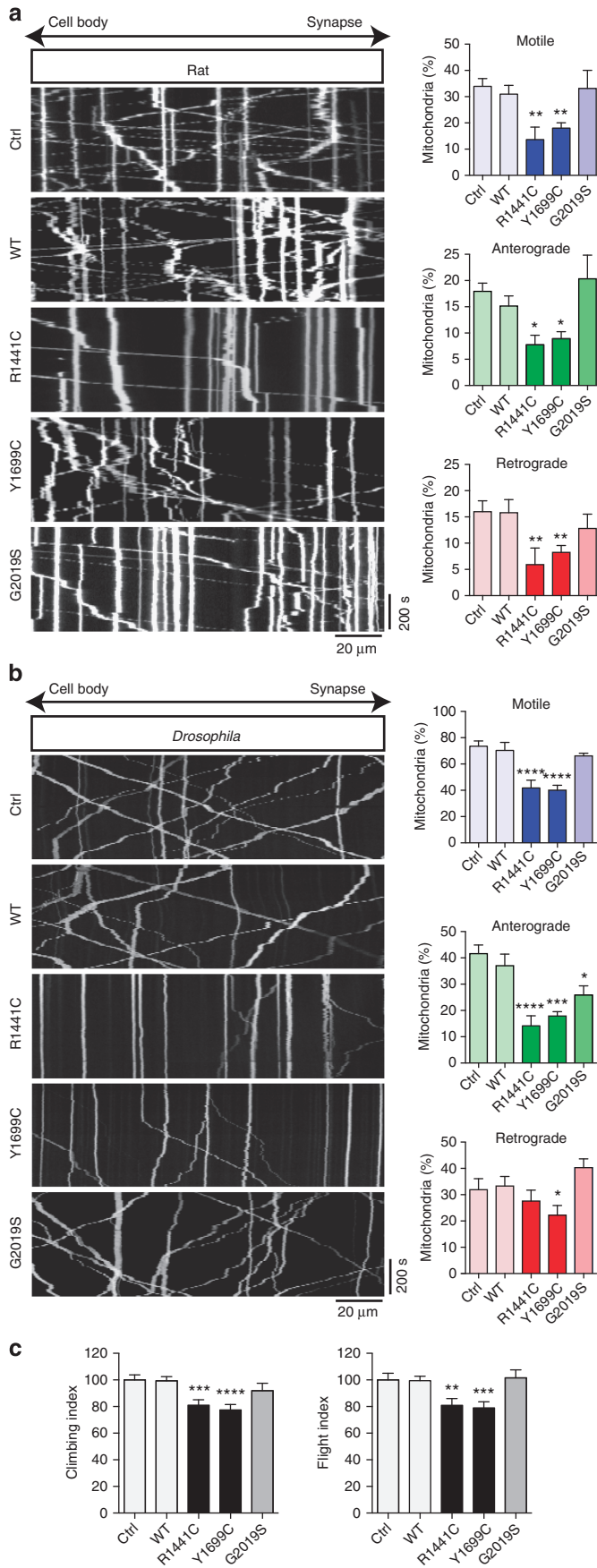
**Roc-COR mutants form filamentous structures on microtubules.** The bidirectional nature of the axonal transport defect suggested the disturbance of a common transport component such as microtubules. It has been reported that *LRRK2* can interact with microtubules and even alter tubulin acetylation<sup>14–18</sup>. Importantly, the acetylation status of microtubules is known to influence the rate of transport along them, with increased acetylation promoting axonal transport<sup>25,26</sup>. Therefore, we hypothesized that *LRRK2* Roc-COR mutants may affect the equilibrium of microtubules. To address this, we analysed the association of *LRRK2* variants with microtubules in mammalian CV1 and HEK293 cells, focusing specifically on acetylated microtubules. In contrast to *LRRK2*-WT, we found that *LRRK2*-R1441C and *LRRK2*-Y1699C had a propensity to form filamentous structures that appeared to align with microtubules (Fig. 2). These structures are reminiscent of previously reported skein-like *LRRK2* structures<sup>17,27</sup>. Furthermore, where *LRRK2*-R1441C or *LRRK2*-Y1699C was present,  $\alpha$ -tubulin acetylation was lacking. These observations are consistent with *LRRK2*-R1441C and *LRRK2*-Y1699C inhibiting axonal transport by interfering with microtubule acetylation.

### Increasing microtubule acetylation inhibits *LRRK2* filaments.

We next investigated whether the interaction of *LRRK2* variants with deacetylated microtubules was reversible and sensitive to microtubule acetylation. We treated CV1 and HEK293 cells with the broad deacetylase inhibitor trichostatin A (TSA), which promotes  $\alpha$ -tubulin acetylation<sup>26</sup>, and analysed filament formation. In both CV1 and HEK293 cells, TSA treatment significantly reduced the formation of filamentous *LRRK2* (Fig. 2).

The family of histone deacetylases (HDACs) is classified into four groups based on function and DNA sequence similarity. Classes I, IIa and IIb are considered the classical HDACs whose activities are inhibited by TSA. Class III comprises a family of NAD<sup>+</sup>-dependent proteins called the Sirtuins (SIRT) that are not affected by TSA. Class IV is an atypical class based solely on DNA sequence similarity to the others. Both the class IIb member HDAC6 and class III member SIRT2 have been shown to deacetylate  $\alpha$ -tubulin<sup>28,29</sup> and conversely their inhibition increases microtubule acetylation. Thus, although in our assays HDAC6 was likely to be the main target of TSA, other pathways could have been affected by TSA treatment. To more selectively target microtubule acetylation, we treated HEK293 cells expressing *LRRK2* Roc-COR mutants with the specific HDAC6 inhibitor tubastatin-A<sup>30–32</sup> or the SIRT2-specific inhibitor AGK2 (ref. 33). Specific inhibition of either HDAC6 or SIRT2 prevented the formation of filamentous *LRRK2* to the same extent as TSA (Fig. 3).

To further characterize the potential role of microtubule acetylation in the *LRRK2* Roc-COR mutant filamentous phenotype, we expressed the  $\alpha$ -tubulin acetyl transferase  $\alpha$ TAT1 (also called MEC17)<sup>34,35</sup>. Because  $\alpha$ -tubulin is the major cellular



substrate of  $\alpha$ TAT1, the overexpression of  $\alpha$ TAT1 specifically increases microtubule acetylation<sup>36</sup>.  $\alpha$ TAT1 expression also significantly reversed the filamentous LRRK2 Roc-COR mutant phenotype (Fig. 4) confirming that microtubule acetylation regulates the association of LRRK2 Roc-COR mutants with microtubules.

Together these findings support previous reports that LRRK2 associates with microtubules and indicate that LRRK2 Roc-COR mutants interfere with  $\alpha$ -tubulin acetylation, which can be restored by the inhibition of the deacetylase enzymes HDAC6 and SIRT2 or by the overexpression of  $\alpha$ TAT1.

**TSA restores axonal transport and locomotion.** Reversal of the association of LRRK2 Roc-COR mutants with deacetylated microtubules prompted us to address whether modulating microtubule acetylation could also reverse the axonal transport defects *in vitro* and *in vivo*. We first targeted the tubulin deacetylases *in vivo* using transgenic *Drosophila HDAC6* or *Sirt2* RNA interference (RNAi) lines. Loss of either *HDAC6* or *Sirt2* effectively restored axonal transport of mitochondria in LRRK2 Roc-COR mutant transgenic flies (Fig. 5a,b). Moreover, the knockdown of *HDAC6* or *Sirt2* was able to significantly rescue climbing and flight deficits caused by mutant LRRK2 (Fig. 5c).

The ability of TSA to prevent mutant LRRK2 from aberrant binding to microtubules makes this an attractive therapeutic intervention. We tested this idea by treating primary rat neurons expressing LRRK2-Y1699C with TSA. Encouragingly, this was able to restore axonal transport to control levels (Fig. 6a). To extend this observation *in vivo*, *Drosophila* expressing the LRRK2 variants were raised on TSA-dosed food. Remarkably, this completely rescued the transport defects caused by LRRK2-R1441C or Y1699C (Fig. 6b). Similarly, transport defects caused by *Lrrk*-R1069C or Y1383C expression were also restored by feeding TSA (Supplementary Fig. 3). Thus, both genetic and pharmacological approaches *in vitro* and *in vivo* show that increasing microtubule acetylation can rescue LRRK2 Roc-COR mutant-induced axonal transport defects.

Finally, we asked whether treatment with TSA would be able to rescue the locomotor deficits cause by the defective axonal transport even after the onset of the phenotype. We took newly emerged flies expressing WT and mutant forms of LRRK2 or *Lrrk* that had been raised on normal food, which as we previously showed already exhibited climbing and flight deficits (Fig. 1c). These young adult flies were then fed TSA for 5 days and tested for locomotion. Notably, even with this modest increase in age, the locomotor deficit had worsened in control-fed animals (Fig. 6c and Supplementary Fig. 3c). However, the administration of TSA was sufficient to fully restore locomotor ability in the

**Figure 1 | LRRK2 Roc-COR domain mutations interfere with axonal transport.** Kymographs show transport of (a) DsRed-labelled mitochondria in rat cortical neurons transfected to express the indicated acGFP1-tagged LRRK2 variants (Control is expressing acGFP1 alone) or (b) mito-GFP-labelled mitochondria in transgenic *Drosophila* motor neurons expressing the indicated LRRK2 variants. Charts are mean  $\pm$  s.e.m. of quantified mitochondrial transport shown as percentage of total mitochondria. (c) Locomotion assays for climbing and flight behaviour of LRRK2 variants expressed in motor neurons by *D42-GAL4*. *Drosophila* control is driver/reporter crossed to a *lacZ* transgene. \* $P < 0.05$ , \*\* $P < 0.01$ , \*\*\* $P < 0.001$ , \*\*\*\* $P < 0.0001$ , one-way analysis of variance followed by Fisher's least significant difference *post hoc* test. (a)  $N$  (cells; from four to eight experiments) = Ctrl, 5; WT, 12; R1441C, 6; Y1699C, 20; G2019S, 7. (b)  $N$  (animals) = Ctrl, 10; WT, 10; R1441C, 12; Y1699C, 14; G2019S, 11. (c)  $N$  (animals) = Ctrl, 95; WT, 141; R1441C, 93; Y1699C, 122; G2019S, 59.



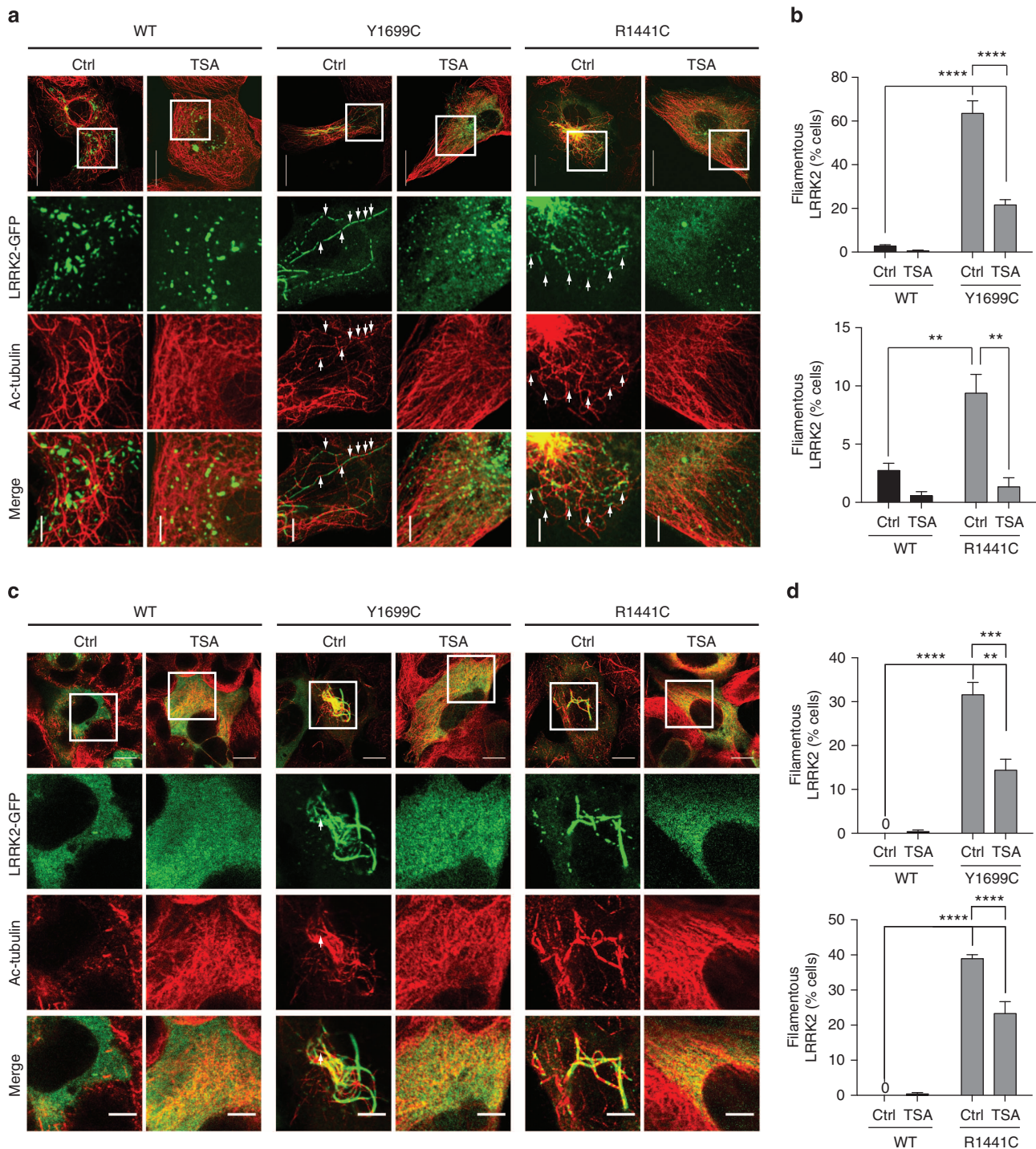


**Figure 2 | LRRK2 Roc-COR domain mutants form TSA-sensitive filamentous structures.** CV1 (**a**) or HEK293 (**c**) cells were transfected with acGFP1-tagged LRRK2 variants (green) as indicated. Twenty-four hours after transfection, the cells were treated with vehicle (Ctrl) or 0.5  $\mu$ M TSA for 4 h. After treatment, the cells were fixed and processed for immunostaining using anti-acetylated  $\alpha$ -tubulin antibody (red). Scale bar, 20  $\mu$ m (**a**), 10  $\mu$ m (**c**); zoom, 5  $\mu$ m. The percentage of vehicle (Ctrl) and TSA-treated (TSA) CV1 (**b**) and HEK293 (**d**) cells exhibiting filamentous LRRK2 was quantified (mean  $\pm$  s.e.m., zero values are indicated (0)). \*\* $P$  < 0.01, \*\*\* $P$  < 0.001, \*\*\*\* $P$  < 0.0001, two-way analysis of variance followed by Fisher's least significant difference *post hoc* test. (**b**)  $N$  (coverslips counted,  $\sim$ 50 cells per coverslip; from four experiments) = WT, 7; WT + TSA, 5; Y1699C, 4; Y1699C + TSA, 5; R1441C, 11; R1441C + TSA, 4. (**d**)  $N$  (coverslips counted,  $\sim$ 50 cells per coverslip; from four experiments) = WT, 5; WT + TSA, 5; Y1699C, 13; Y1699C + TSA, 5; R1441C, 15; R1441C + TSA, 5.

LRRK2-R1441C- or Y1699C- and *Lrrk*-R1069C- or Y1383C-expressing animals (Fig. 6c and Supplementary Fig. 3c).

These results demonstrate that increasing microtubule acetylation either genetically by knockdown of deacetylase

enzymes or by systemic administration of a deacetylase inhibitor is sufficient to restore a primary cellular defect and reverse the associated behavioural disruption, even after the onset of behavioural symptoms.

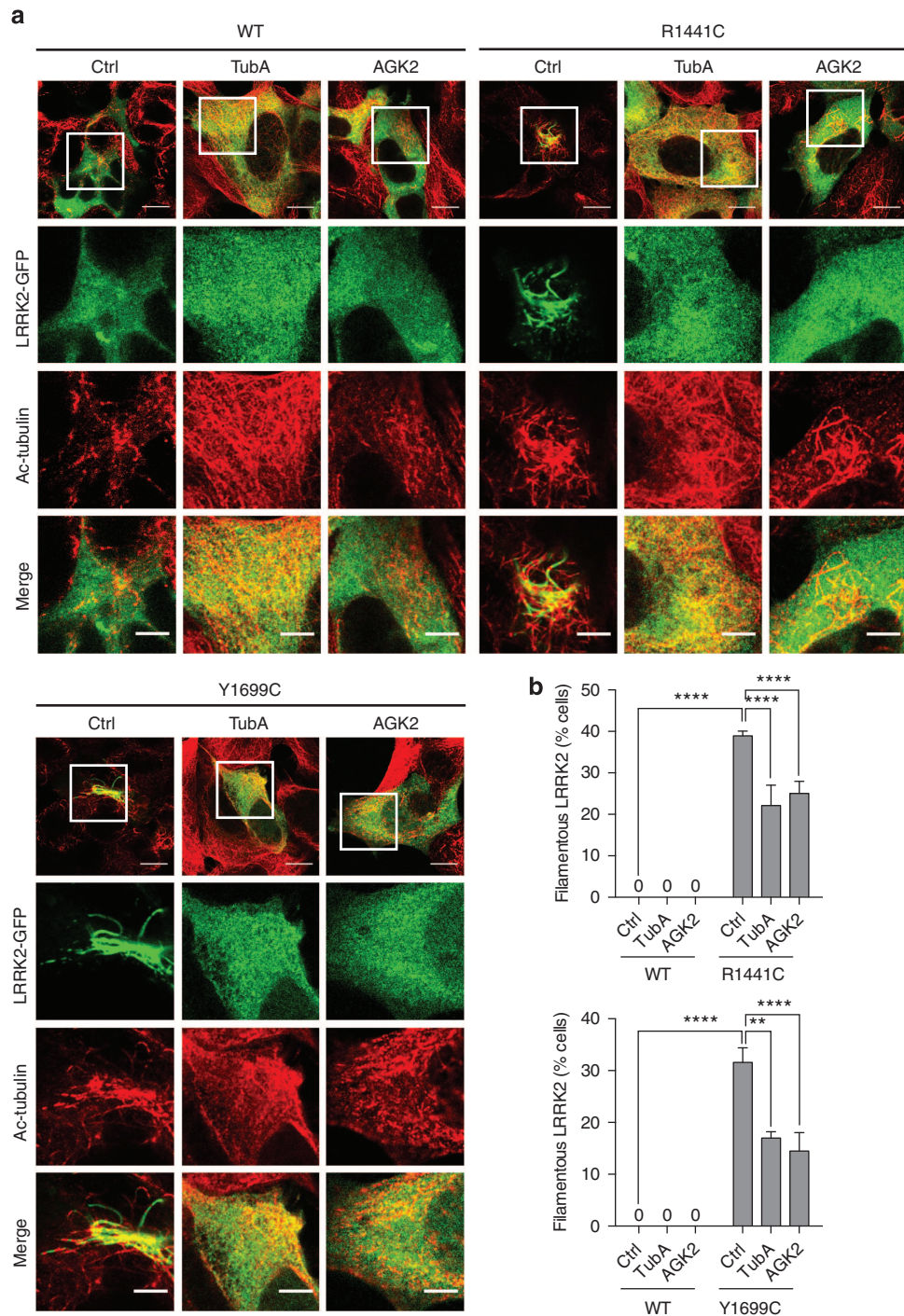


**Figure 3 | Both HDAC6 and SIRT2 inhibitors prevent LRRK2 Roc-COR mutant filamentous structures.** (a) HEK293 cells were transfected with acGFP1-tagged LRRK2 variants (green) as indicated. Twenty-four hours after transfection, the cells were treated with vehicle (Ctrl), 2  $\mu$ M tubastatin-A (TubA) or 5  $\mu$ M AGK2 for 4 h. After treatment, the cells were fixed and processed for immunostaining using anti-acetylated  $\alpha$ -tubulin antibody (red). Scale bar, 10  $\mu$ m; zoom, 5  $\mu$ m. (b) The percentage of vehicle (Ctrl), TubA and AGK2-treated HEK293 cells exhibiting filamentous LRRK2 was quantified (mean  $\pm$  s.e.m., zero values are indicated (0)).  $^{**}P < 0.01$ ,  $^{****}P < 0.0001$ , two-way analysis of variance followed by Fisher's least significant difference *post hoc* test. *N* (coverslips counted,  $\sim$ 50 cells per coverslip, from four experiments) = WT, 5; WT + TubA, 5; WT + AGK2, 5; Y1699C, 13; Y1699C + TubA, 4; Y1699C + AGK2, 9; R1441C, 15; R1441C + TubA, 5; R1441C + AGK2, 9.

**Discussion**

Disruption of axonal transport is an early feature in a number of neurodegenerative diseases including PD<sup>19</sup>. Analysis of axonal transport of WT and pathogenic mutants of  $\alpha$ -synuclein have revealed reduced transport rates of the mutants, which may contribute to the formation of Lewy bodies<sup>21</sup>. PINK1 and

Parkin, mutations in which cause the majority of early-onset recessive familial PD<sup>37,38</sup>, have been shown to directly affect mitochondrial transport<sup>23,24</sup> and this in turn regulates mitophagy<sup>39</sup>. Halting of axonal transport has also been observed in mitochondrial neurotoxin models of sporadic PD<sup>40-42</sup>.



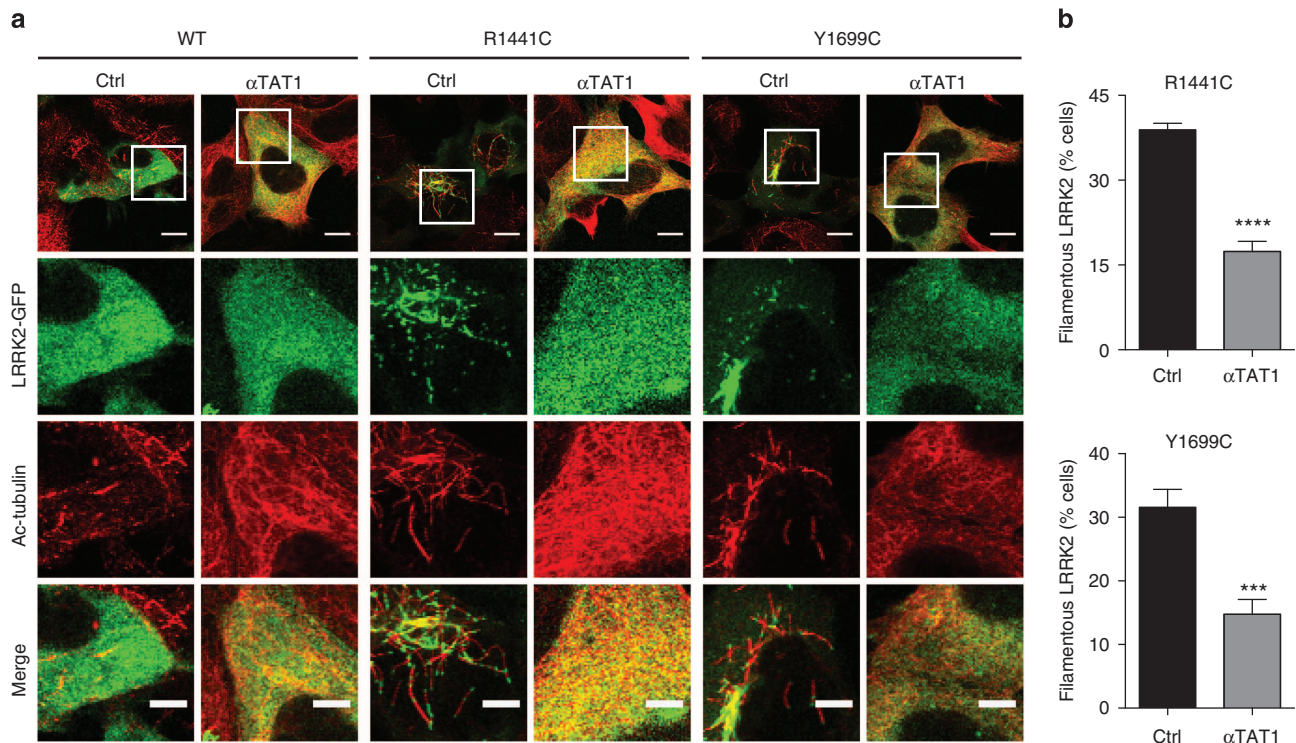


**Figure 4 |  $\alpha$ TAT1 expression prevents LRRK2 Roc-COR mutant filamentous structures.** (a) HEK293 cells were co-transfected with acGFP1-tagged LRRK2 variants (green) and either empty vector (Ctrl) or  $\alpha$ TAT1 as indicated ( $3 \times$  excess of empty vector or  $\alpha$ TAT1 was used to ensure co-transfection). Twenty-four hours after transfection, the cells were fixed and processed for immunostaining using anti-acetylated  $\alpha$ -tubulin antibody (red). Scale bar, 10  $\mu$ m; zoom, 5  $\mu$ m. (b) The percentage of empty vector- (Ctrl) and  $\alpha$ TAT1-transfected HEK293 cells exhibiting filamentous LRRK2 was quantified (mean  $\pm$  s.e.m.). \*\*\* $P$  < 0.001, \*\*\*\* $P$  < 0.0001, Student's  $t$ -test,  $N$  (coverslips counted,  $\sim$  50 cells per coverslip; from four experiments) = WT, 5; WT +  $\alpha$ TAT1, 5; Y1699C, 13; Y1699C +  $\alpha$ TAT1, 13; R1441C, 15; R1441C +  $\alpha$ TAT1, 13.

In this study, we investigated whether PD-associated mutations in LRRK2 affect axonal transport and cause dysfunction of the motor system. We found that pathogenic mutations in the Roc-COR domain of LRRK2 (R1441C and Y1699C) disrupt axonal transport of mitochondria *in vitro* in cultured neurons and *in vivo*, and cause locomotor deficits in *Drosophila*. The effects are evolutionarily conserved since the expression of mutant *Drosophila Lrrk* variants also inhibited transport and motor ability.

LRRK2 has been shown to interact with microtubules but the physiological relevance of this interaction is poorly understood<sup>14–18</sup>. We found that both LRRK2-R1441C and Y1699C mutants, but not LRRK2-WT, formed filament-like structures that decorated deacetylated microtubules. Previous work has shown that acetylation of microtubules regulates axonal transport<sup>25,26</sup> and has implicated LRRK2 in the regulation of microtubule acetylation<sup>18</sup>. We therefore increased microtubule acetylation using pharmacological inhibitors or RNAi knockdown of the deacetylase enzymes HDAC6 and SIRT2, or by the expression of  $\alpha$ TAT1 and found that this prevented the decoration of microtubules by LRRK2-R1441C and Y1699C. Importantly, increasing microtubule acetylation restored axonal transport to WT levels *in vitro* and *in vivo*.

Interestingly the kinase domain mutant LRRK2-G2019S did not affect axonal transport. Several groups have shown that the R1441C and Y1699C mutations inhibit the GTPase activity of LRRK2 but have normal kinase activity<sup>6,7,43,44</sup>, whereas LRRK2-G2019S has increased kinase activity but normal GTPase activity compared with WT LRRK2 (refs 8,9,45,46). Thus, our results suggest that the inhibition of axonal transport is likely linked to decreased LRRK2 GTPase activity. This is in line with increasing

evidence suggesting that the GTPase activity of LRRK2 plays an important role in pathogenesis<sup>47</sup>. Interestingly, the pharmacological inhibition of LRRK2 kinase activity has been shown to induce a redistribution of LRRK2 that appears similar to the microtubule-attached distribution we observed with LRRK2 Roc-COR mutants<sup>48</sup> and the binding of LRRK2 to tubulin was significantly enhanced by LRRK2 kinase inhibition in an indirect reporter assay<sup>16</sup>. However, since the LRRK2 Roc-COR mutants analysed here have normal kinase activity<sup>6,7,43,44</sup>, our data suggest that the GTPase activity of LRRK2 plays a key role in LRRK2's interaction with microtubules. The effect of LRRK2 kinase inhibitors may be explained by a model in which LRRK2 kinase regulates the GTPase via phosphorylation<sup>47</sup>.

The *Drosophila* model allowed us to extend our observations of defective axonal transport in a number of ways. First, it allowed us to address whether the inhibition of axonal transport by LRRK2 Roc-COR mutants had any physiological consequences in adult motor behaviours. We found that *Drosophila* expressing LRRK2 Roc-COR mutants also resulted in a deficit of the motor system, causing a decrease in both climbing and flight ability. Furthermore, when we restored axonal transport by increasing microtubule acetylation using HDAC6 or Sirt2 RNAi, this also restored normal locomotor ability. Thus, these results argue that inhibition of axonal transport can cause functional deficits *in vivo*.

Second, this system also enabled us to assess whether pharmacological restoration of acetylated microtubules could reverse the locomotor phenotype after the onset of locomotor symptoms. Indeed, we found that the systemic administration of TSA was able to fully restore locomotor ability, showing that the effects of the LRRK2 Roc-COR mutants are reversible and, at least

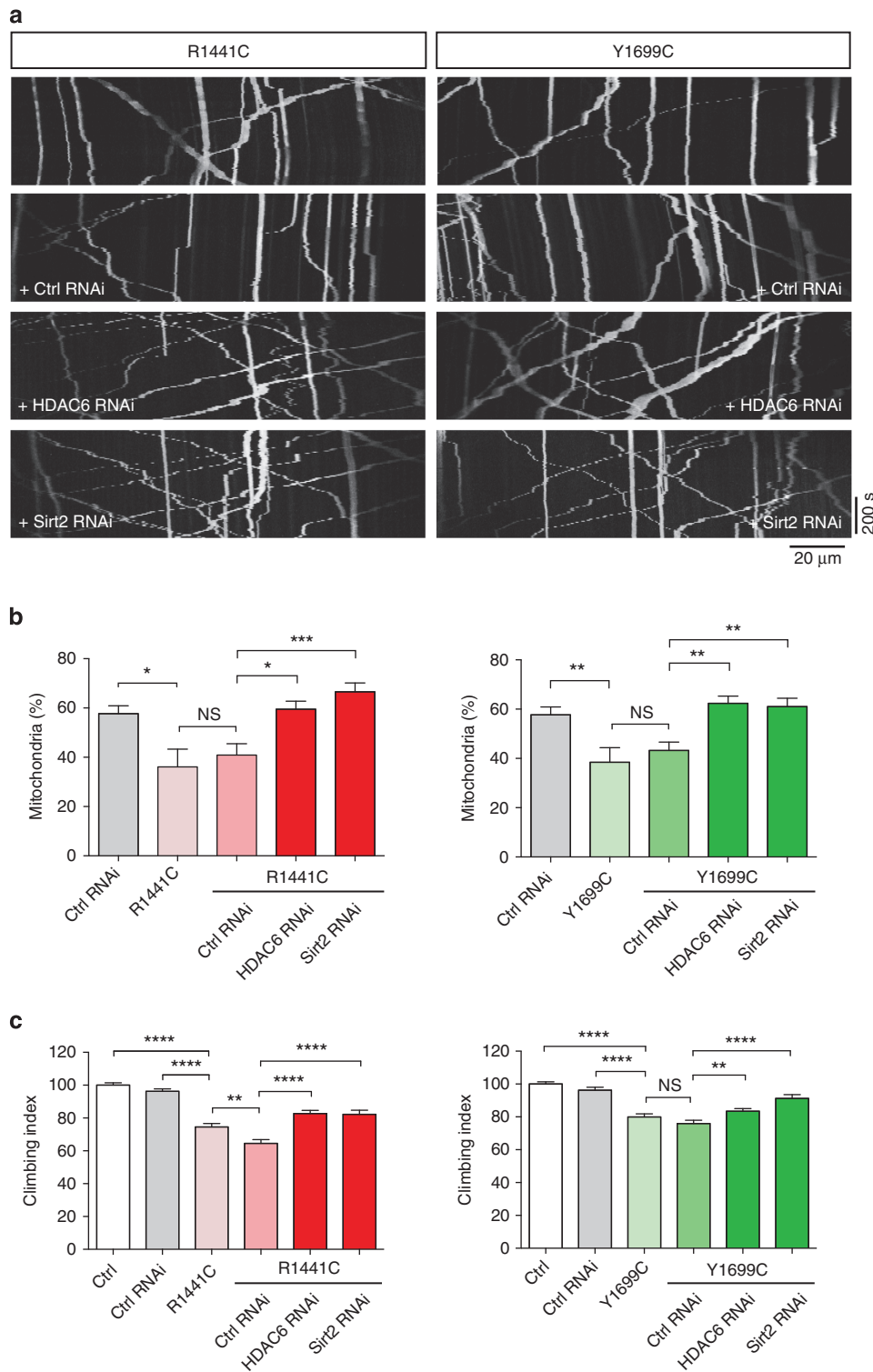
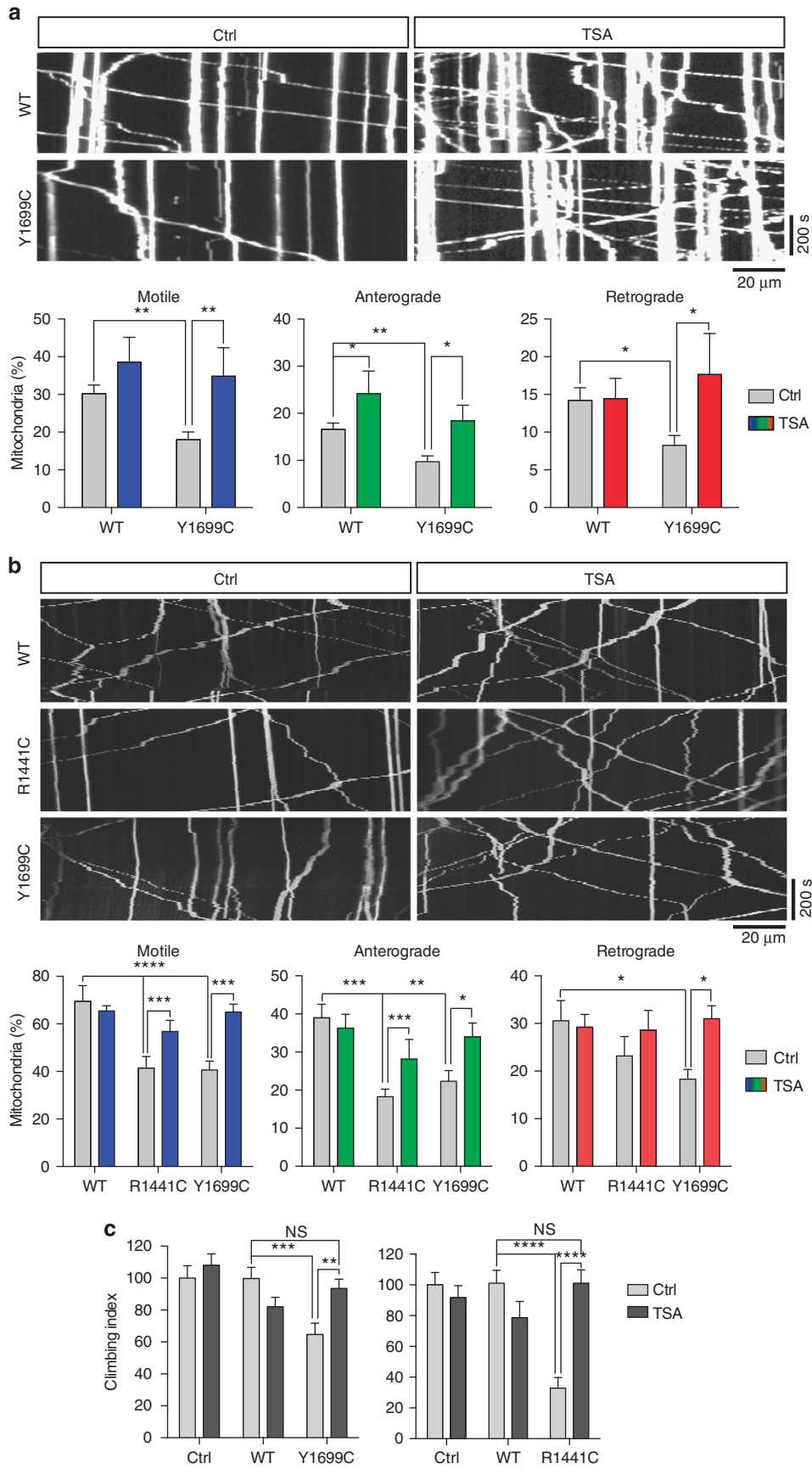


**Figure 5 | HDAC6 and Sirt2 RNAi restores axonal transport and locomotion.** (a) Kymographs of mitochondria in transgenic *Drosophila* motor neurons expressing mito-GFP with indicated LRRK2 variants alone (top) or in combination with HDAC6 or Sirt2 RNAi transgenes. Ctrl RNAi is expressing a *lacZ*-RNAi transgene. (b) Charts are mean  $\pm$  s.e.m. of quantified mitochondrial transport shown as percentage of total mitochondria. (c) Locomotion assays for climbing behavior of indicated genotypes. Transgene expression is driven by *D42-GAL4*. Ctrl is driver crossed to a *lacZ* transgene. \* $P < 0.05$ , \*\* $P < 0.01$ , \*\*\* $P < 0.001$ , \*\*\*\* $P < 0.0001$ , one-way analysis of variance followed by Fisher's least significant difference *post hoc* test. (b) left chart: *N* (animals) = Ctrl RNAi, 11; R1441C, 9; R1441C + Ctrl RNAi, 23; R1441C + HDAC6 RNAi, 13; R1441C + Sirt2 RNAi, 12; right chart: *N* (animals) = Ctrl RNAi, 11; Y1699C, 11; Y1699C + Ctrl RNAi, 13; Y1699C + HDAC6 RNAi, 15; Y1699C + Sirt2 RNAi, 18. (c) left chart: *N* (animals) = Ctrl, 379; Ctrl RNAi, 326; R1441C, 367; R1441C + Ctrl RNAi, 245; R1441C + HDAC6 RNAi, 300; R1441C + Sirt2 RNAi, 218; right chart: *N* (animals) = Ctrl, 329; Ctrl RNAi, 281; Y1699C, 381; Y1699C + Ctrl RNAi, 338; Y1699C + HDAC6 RNAi, 413; Y1699C + Sirt2 RNAi, 170.





in the fly, are amenable to *post hoc* treatment. Thus, our study adds PD to the growing list of neurodegenerative diseases that involve disturbed axonal transport in which deacetylase inhibitors have been shown to confer protection including Charcot-Marie-Tooth disease, Alzheimer's disease, amyotrophic lateral sclerosis and Huntington's disease<sup>26,49–55</sup>.

In conclusion, our results reveal that mutant LRRK2-associated PD involves defective axonal transport and suggest that treating with deacetylase inhibitors to restore transport may have therapeutic potential.

## Methods

**Plasmids.** pAcGFP1-LRRK2-WT, Y1699C and R1441C variants were a gift from M. Cookson (NIH, Bethesda). pAcGFP1-LRRK2-G2019S was generated by mutagenesis of pAcGFP1-LRRK2-WT using a QuikChange Site-Directed Mutagenesis Kit (Stratagene) according to the manufacturer's instructions. Mutagenic primers were: 5'-caaaattgctgactacagctgctcagctactgctg-3' (forward) and 5'-cagcagctactgacgaatgctgctgctgacgaatctttg-3' (reverse). Mutagenesis was verified by sequencing. The pSPORT6-MEC17 ( $\alpha$ TAT1) expression plasmid has been described<sup>35</sup> and was a gift from J. Gaertig (University of Georgia, Athens, GA).

**Cell culture and plasmid transfection.** CV1 and HEK293 cells obtained from the ATCC were maintained in Dulbecco's modified Eagle's medium (Invitrogen) containing 4.5 g l<sup>-1</sup> glucose, 10% foetal bovine serum (Sera Laboratories), 2 mM L-glutamine (Invitrogen) and 1 mM sodium pyruvate (Sigma) and were transfected using Exgen500 (Fermentas) or Lipofectamine 2000 (Invitrogen) according to the manufacturer's instructions. All cells were used in experiments 16–24 h post transfection.

Cortical neurons were isolated and transfected as previously described<sup>56–59</sup>. Briefly, cortical neurons were isolated from embryonic day 18 rat embryos and cultured on glass coverslips coated with poly-L-lysine in six or 12-well plates in neurobasal medium containing B27 supplement (Invitrogen), 100 IU ml<sup>-1</sup> penicillin, 100  $\mu$ g ml<sup>-1</sup> streptomycin and 2 mM L-glutamine. Cells were cultured for 7 days and then transfected using a calcium phosphate Protection kit (Promega). For studies on the effects of LRRK2 on axonal transport, neurons were transfected with twice the amount of LRRK2 plasmid compared with DsRed-Mito to ensure that all cells visualized for mitochondrial transport expressed LRRK2 and this was confirmed by AcGFP1 fluorescence.

**Antibodies.** Anti-acetylated  $\alpha$ -tubulin mouse monoclonal antibody was from Sigma (clone 6-11B-1) and used diluted 1:5,000. Secondary antibodies were Alexa fluorophore(546 and 633)-coupled goat anti-mouse IgG from Invitrogen (dilution 1:500).

## Immunofluorescence analysis of LRRK2 microtubule interaction.

Immunostaining was performed as described previously<sup>60</sup>. Briefly, CV1 or HEK293 cells on glass coverslips were fixed with 3.7% formaldehyde in PBS for 20 min at room temperature. After washing with PBS, residual formaldehyde was quenched by incubation with 50 mM NH<sub>4</sub>Cl in PBS for 15 min at room temperature, followed by a second round of washing with PBS. Subsequently, the cells were permeabilized with -20 °C MeOH for 20 min or by incubation with 0.2% Triton-X-100 in PBS for 3 min. MeOH or Triton-X-100 was removed by washing with PBS.

After fixing, the cells were incubated with PBS containing 0.2% fish gelatine (PBS/F) for 30 min at room temperature and then with the primary antibody in PBS/F for 1 h. After washing with PBS/F, the cells were incubated with secondary antibody in PBS/F for 45 min at room temperature. After a final wash, the samples were mounted in Moviol (Calbiochem) containing 1% DABCO or Dako fluorescence mounting medium.

Confocal images were recorded with an LSM510Meta (Carl Zeiss) or a Leica SP5 (Leica Microsystems) confocal microscope using a  $\times 63$ , 1.4NA objective.

**Axonal transport of mitochondria in rat cortical neurons.** Live microscopy of mitochondrial axonal transport in cortical neurons was performed with an Axiovert S100 microscope (Carl Zeiss) equipped with a Lambda LS Xenon-Arc light source (Sutter Instrument Company, Novato, CA), an EGFP/DsRed filterset (Chroma Technology Corp.),  $\times 40$  EC Plan-Neofluar 1.3 N.A. objective (Zeiss), Lambda 10-3 filter wheel (Sutter Instrument Co.) and a Photometrics Cascade-II 512B High Speed EMCCD camera (Photometrics). Post transfection (36–48 h), neurons on coverslips were transferred to a custom observation chamber mounted on the stage of the microscope. The cells were maintained at 37 °C using an objective heater (Tempcontrol 37-2, Carl Zeiss) and 'The Box' Microscope Temperature Control System (Life Imaging Systems). Mitochondrial movements were recorded for 10 min with 3 s time-lapse interval using Metamorph software (Molecular Devices).

Image analysis was performed with ImageJ developed by Wayne Rasband (NIH, Bethesda, USA; <http://rsb.info.nih.gov/ij/>) extended with custom plug-ins, or Metamorph. Calculations of mitochondrial transport parameters were as described before<sup>57,59</sup> except that the overall transport of mitochondria in Figs 1 and 5 were analysed from kymographs using the SlopeToVelocity plugin described previously<sup>59</sup>. Briefly, this plugin calculates the velocity by measuring the distance between the position of individual mitochondria at the start and end of time-lapse recordings and dividing by the time elapsed. This yields an overall velocity of transport that includes anterograde and retrograde movements and stationary periods. Mitochondria were subsequently classified as motile (velocity  $> 0.1 \mu\text{m s}^{-1}$ ) or stationary (velocity  $\leq 0.1 \mu\text{m s}^{-1}$ ).

**Drosophila stocks and procedures.** *Drosophila* were raised under standard conditions at 25 °C on agar, cornmeal and yeast food. Transgenic lines used were: UAS-LRRK2 WT<sup>61</sup>, UAS-LRRK2 R1441C<sup>62</sup>, UAS-LRRK2 Y1699C<sup>63</sup>, UAS-LRRK2 G2019S<sup>61</sup>, UAS-Lrrk WT<sup>64</sup>, UAS-Lrrk R1069C<sup>64</sup> and UAS-Lrrk Y1383C<sup>63</sup>. D42-GAL4, CCAP-GAL4, UAS-mitoGFP and UAS-lacZ were obtained from the Bloomington Drosophila Stock Center. UAS-lacZ-RNAi (#51446), UAS-HDAC6-RNAi (#108831) and UAS-Sirt2-RNAi (#21999) were obtained from the Vienna Drosophila Resource Centre<sup>65</sup>. Flight and climbing assays were performed as previously described<sup>66</sup>.

**Dissection and imaging of axonal transport in Drosophila.** Live dissections of wandering third instar larvae were performed as previously described<sup>67</sup>. Individual larvae were placed on Sylgard slide and pinned on both ends with the dorsal side up. Larval body wall muscles were carefully opened using microdissection scissors. Internal organs were removed with forceps without disturbing the ventral ganglion and motor neurons. The cuticle was laterally expanded on both sides and pinned. The whole preparation was washed in 1 ml dissecting buffer containing 128 mM NaCl, 1 mM EGTA, 4 mM MgCl<sub>2</sub>, 2 mM KCl, 5 mM HEPES and 36 mM sucrose, pH 7.2. The buffer was replaced and the larvae kept immersed in buffer during imaging. Imaging was done on an Olympus FV1000 confocal using  $\times 60$  water immersion objective (NA 0.90, Olympus LUMPLFL). Time-lapse movies were acquired at the rate of 1 frame per 5 s for 500 s. A minimum of 10 movies (one movie per larva) were taken for each genotype/treatment.

**Analysis of mitochondrial movement in Drosophila.** All movies were analysed using ImageJ software. The movies were processed in ImageJ and kymographs were generated as previously described<sup>59</sup>. Using kymographs, the number of mitochondria moving in anterograde and retrograde directions were quantified along with the number of stationary mitochondria. Mitochondria were scored as moving if the organelle is in motion for at least 60% of the movie. All scoring was performed blind to the experimental condition.

**Drug treatment in Drosophila.** Crosses were raised in standard medium supplemented with 10  $\mu$ M TSA (Sigma-Aldrich T8552). Dimethylsulphoxide (0.06%) was used as a control. For adult climbing, crosses with D42-GAL4 were raised in standard medium and young progeny of 1–2 days were collected. Flies were starved in empty vials for 3–4 h at 25 °C and then placed in vials with filter papers soaked with 1 ml solution containing 10% sucrose and 100  $\mu$ M TSA<sup>68</sup>. Dimethylsulphoxide

**Figure 6 | Axonal transport and locomotion is restored by TSA treatment.** (a) Kymographs show transport of DsRed-labelled mitochondria in rat cortical neurons transfected with acGFP1-tagged LRRK2 variants as indicated and treated with vehicle (Ctrl) or 0.5  $\mu$ M TSA for 4 h. Charts are mean  $\pm$  s.e.m. of quantified mitochondrial transport shown as percentage of total mitochondria. (b) Kymographs of mitochondria in transgenic *Drosophila* motor neurons expressing mito-GFP and indicated LRRK2 variants. Ctrl is expressing a *lacZ* transgene. *Drosophila* were raised on food containing vehicle control (Ctrl) or 10  $\mu$ M TSA. Charts are mean  $\pm$  s.e.m. of quantified mitochondrial transport shown as percentage of total mitochondria. (c) Locomotion assays for climbing behavior following vehicle control or TSA treatment. *Drosophila* were raised on normal food, then fed vehicle (Ctrl) or TSA supplemented food for 5 days before testing. Transgene expression is driven by D42-GAL4. \* $P < 0.05$ , \*\* $P < 0.01$ , \*\*\* $P < 0.001$ , \*\*\*\* $P < 0.0001$ , two-way analysis of variance followed by Fisher's least significant difference *post hoc* test. (a)  $N$  (cells; from three to five experiments) = WT Ctrl, 30; WT TSA, 7; Y1699C Ctrl, 20; Y1699C TSA, 5; (b)  $N$  (animals) = WT Ctrl, 10; WT + TSA, 10; R1441C Ctrl, 13; R1441C + TSA, 13; Y1699C Ctrl, 11; Y1699C + TSA, 11; (c), right chart:  $N$  (animals) = Ctrl Ctrl, 84; Ctrl + TSA, 77; WT Ctrl, 68; WT + TSA, 46; R1441C Ctrl, 43; R1441C + TSA, 53; left chart:  $N$  (animals) = Ctrl Ctrl, 41; Ctrl + TSA, 45; WT Ctrl, 56; WT + TSA, 78; Y1699C Ctrl, 59; Y1699C + TSA, 87.

(0.6%) was used as a control. The filter papers were checked every day and replaced after 48 h. Climbing assays were performed after 5 days, that is, animals were 6–7 days old.

**Statistical analysis.** Calculations and statistical analysis were performed using Excel (Microsoft Corporation, Redmond, WA), and Prism software (GraphPad Software, Inc., San Diego, CA). Statistical significance was determined by one-way or two-way analysis of variance (ANOVA) followed by Fisher's least significant difference *post hoc* test or by *t*-test as indicated in the figure legends.

## References

- Paisan-Ruiz, C. *et al.* Cloning of the gene containing mutations that cause PARK8-linked Parkinson's disease. *Neuron* **44**, 595–600 (2004).
- Zimprich, A. *et al.* Mutations in LRRK2 cause autosomal-dominant parkinsonism with pleomorphic pathology. *Neuron* **44**, 601–607 (2004).
- Gilks, W. P. *et al.* A common LRRK2 mutation in idiopathic Parkinson's disease. *Lancet* **365**, 415–416 (2005).
- Satake, W. *et al.* Genome-wide association study identifies common variants at four loci as genetic risk factors for Parkinson's disease. *Nat. Genet.* **41**, 1303–1307 (2009).
- Simon-Sanchez, J. *et al.* Genome-wide association study reveals genetic risk underlying Parkinson's disease. *Nat. Genet.* **41**, 1308–1312 (2009).
- Guo, L. *et al.* The Parkinson's disease-associated protein, leucine-rich repeat kinase 2 (LRRK2), is an authentic GTPase that stimulates kinase activity. *Exp. Cell Res.* **313**, 3658–3670 (2007).
- Lewis, P. A. *et al.* The R1441C mutation of LRRK2 disrupts GTP hydrolysis. *Biochem. Biophys. Res. Commun.* **357**, 668–671 (2007).
- Greggio, E. *et al.* Kinase activity is required for the toxic effects of mutant LRRK2/dardarin. *Neurobiol. Dis.* **23**, 329–341 (2006).
- Jaleel, M. *et al.* LRRK2 phosphorylates moesin at threonine-558: characterization of how Parkinson's disease mutants affect kinase activity. *Biochem. J.* **405**, 307–317 (2007).
- Cookson, M. R. Cellular effects of LRRK2 mutations. *Biochem. Soc. Trans.* **40**, 1070–1073 (2012).
- MacLeod, D. *et al.* The familial Parkinsonism gene LRRK2 regulates neurite process morphology. *Neuron* **52**, 587–593 (2006).
- Parisiadou, L. *et al.* Phosphorylation of ezrin/radixin/moesin proteins by LRRK2 promotes the rearrangement of actin cytoskeleton in neuronal morphogenesis. *J. Neurosci.* **29**, 13971–13980 (2009).
- Plowey, E. D., Cherra, 3rd S. J., Liu, Y. J. & Chu, C. T. Role of autophagy in G2019S-LRRK2-associated neurite shortening in differentiated SH-SY5Y cells. *J. Neurochem.* **105**, 1048–1056 (2008).
- Gillardon, F. Interaction of elongation factor 1- $\alpha$  with leucine-rich repeat kinase 2 impairs kinase activity and microtubule bundling *in vitro*. *Neuroscience* **163**, 533–539 (2009).
- Gillardon, F. Leucine-rich repeat kinase 2 phosphorylates brain tubulin- $\beta$  isoforms and modulates microtubule stability—a point of convergence in parkinsonian neurodegeneration? *J. Neurochem.* **110**, 1514–1522 (2009).
- Caesar, M. *et al.* Leucine-rich repeat kinase 2 functionally interacts with microtubules and kinase-dependently modulates cell migration. *Neurobiol. Dis.* **54**, 280–288 (2013).
- Kett, L. R. *et al.* LRRK2 Parkinson disease mutations enhance its microtubule association. *Hum. Mol. Genet.* **21**, 890–899 (2012).
- Law, B. M. *et al.* A direct interaction between leucine-rich repeat kinase 2 and specific  $\beta$ -tubulin isoforms regulates tubulin acetylation. *J. Biol. Chem.* **289**, 895–908 (2014).
- De Vos, K. J., Grierson, A. J., Ackerley, S. & Miller, C. C. J. Role of axonal transport in neurodegenerative diseases. *Annu. Rev. Neurosci.* **31**, 151–173 (2008).
- Liu, S. *et al.* Parkinson's disease-associated kinase PINK1 regulates Miro protein level and axonal transport of mitochondria. *PLoS Genet.* **8**, e1002537 (2012).
- Saha, A. R. *et al.* Parkinson's disease alpha-synuclein mutations exhibit defective axonal transport in cultured neurons. *J. Cell Sci.* **117**, 1017–1024 (2004).
- Chu, Y. *et al.* Alterations in axonal transport motor proteins in sporadic and experimental Parkinson's disease. *Brain* **135**, 2058–2073 (2012).
- Wang, X. *et al.* PINK1 and Parkin target Miro for phosphorylation and degradation to arrest mitochondrial motility. *Cell* **147**, 893–906 (2011).
- Weihofen, A., Thomas, K. J., Ostaszewski, B., Cookson, M. & Selkoe, D. J. Pink1 forms a multi-protein complex with Miro and Milton, linking Pink1 function to mitochondrial trafficking. *Biochemistry* **48**, 2045–2052 (2009).
- Reed, N. A. *et al.* Microtubule acetylation promotes kinesin-1 binding and transport. *Curr. Biol.* **16**, 2166–2172 (2006).
- Dompierre, J. P. *et al.* Histone deacetylase 6 inhibition compensates for the transport deficit in Huntington's disease by increasing tubulin acetylation. *J. Neurosci.* **27**, 3571–3583 (2007).
- Alegre-Abarrategui, J. *et al.* LRRK2 regulates autophagic activity and localizes to specific membrane microdomains in a novel human genomic reporter cellular model. *Hum. Mol. Genet.* **18**, 4022–4034 (2009).
- Hubbert, C. *et al.* HDAC6 is a microtubule-associated deacetylase. *Nature* **417**, 455–458 (2002).
- Southwood, C. M., Peppi, M., Dryden, S., Tainsky, M. A. & Gow, A. Microtubule deacetylases, SirT2 and HDAC6, in the nervous system. *Neurochem. Res.* **32**, 187–195 (2007).
- Haggarty, S. J., Koeller, K. M., Wong, J. C., Grozinger, C. M. & Schreiber, S. L. Domain-selective small-molecule inhibitor of histone deacetylase 6 (HDAC6)-mediated tubulin deacetylation. *Proc. Natl Acad. Sci. USA* **100**, 4389–4394 (2003).
- Butler, K. V. *et al.* Rational design and simple chemistry yield a superior, neuroprotective HDAC6 inhibitor, tubastatin A. *J. Am. Chem. Soc.* **132**, 10842–10846 (2010).
- Hu, E. *et al.* Identification of novel isoform-selective inhibitors within class I histone deacetylases. *J. Pharmacol. Exp. Ther.* **307**, 720–728 (2003).
- Outeiro, T. F. *et al.* Sirtuin 2 inhibitors rescue alpha-synuclein-mediated toxicity in models of Parkinson's disease. *Science* **317**, 516–519 (2007).
- Shida, T., Cueva, J. G., Xu, Z., Goodman, M. B. & Nachury, M. V. The major alpha-tubulin K40 acetyltransferase alphaTAT1 promotes rapid cilogenesis and efficient mechanosensation. *Proc. Natl Acad. Sci. USA* **107**, 21517–21522 (2010).
- Akella, J. S. *et al.* MEC-17 is an alpha-tubulin acetyltransferase. *Nature* **467**, 218–222 (2010).
- Kalebic, N. *et al.* Tubulin acetyltransferase alphaTAT1 destabilizes microtubules independently of its acetylation activity. *Mol. Cell. Biol.* **33**, 1114–1123 (2013).
- Kitada, T. *et al.* Mutations in the parkin gene cause autosomal recessive juvenile parkinsonism. *Nature* **392**, 605–608 (1998).
- Valente, E. M. *et al.* Hereditary early-onset Parkinson's disease caused by mutations in PINK1. *Science* **304**, 1158–1160 (2004).
- Cai, Q., Zakaria, H. M., Simone, A. & Sheng, Z. H. Spatial parkin translocation and degradation of damaged mitochondria via mitophagy in live cortical neurons. *Curr. Biol.* **22**, 545–552 (2012).
- Cartelli, D. *et al.* Microtubule dysfunction precedes transport impairment and mitochondria damage in MPP-induced neurodegeneration. *J. Neurochem.* **115**, 247–258 (2010).
- Morfini, G. *et al.* 1-Methyl-4-phenylpyridinium affects fast axonal transport by activation of caspase and protein kinase C. *Proc. Natl Acad. Sci. USA* **104**, 2442–2447 (2007).
- Kim-Han, J. S., Antenor-Dorsey, J. A. & O'Malley, K. L. The parkinsonian mimetic, MPP+, specifically impairs mitochondrial transport in dopamine axons. *J. Neurosci.* **31**, 7212–7221 (2011).
- Li, X. *et al.* Leucine-rich repeat kinase 2 (LRRK2)/PARK8 possesses GTPase activity that is altered in familial Parkinson's disease R1441C/G mutants. *J. Neurochem.* **103**, 238–247 (2007).
- Daniels, V. *et al.* Insight into the mode of action of the LRRK2 Y1699C pathogenic mutant. *J. Neurochem.* **116**, 304–315 (2011).
- West, A. B. *et al.* Parkinson's disease-associated mutations in LRRK2 link enhanced GTP-binding and kinase activities to neuronal toxicity. *Hum. Mol. Genet.* **16**, 223–232 (2007).
- West, A. B. *et al.* Parkinson's disease-associated mutations in leucine-rich repeat kinase 2 augment kinase activity. *Proc. Natl Acad. Sci. USA* **102**, 16842–16847 (2005).
- Taymans, J. M. The GTPase function of LRRK2. *Biochem. Soc. Trans.* **40**, 1063–1069 (2012).
- Dzambo, N. *et al.* Inhibition of LRRK2 kinase activity leads to dephosphorylation of Ser(910)/Ser(935), disruption of 14-3-3 binding and altered cytoplasmic localization. *Biochem. J.* **430**, 405–413 (2010).
- Chen, S., Owens, G. C., Makarenkova, H. & Edelman, D. B. HDAC6 Regulates mitochondrial transport in hippocampal neurons. *PLoS ONE* **5**, e10848 (2010).
- d'Ydewalle, C., Bogaert, E. & Van Den Bosch, L. HDAC6 at the intersection of neuroprotection and neurodegeneration. *Traffic* **13**, 771–779 (2012).
- Kim, C. *et al.* HDAC6 inhibitor blocks amyloid beta-induced impairment of mitochondrial transport in hippocampal neurons. *PLoS ONE* **7**, e42983 (2012).
- Govindarajan, N. *et al.* Reducing HDAC6 ameliorates cognitive deficits in a mouse model for Alzheimer's disease. *EMBO Mol. Med.* **5**, 52–63 (2013).
- Simoes-Pires, C. *et al.* HDAC6 as a target for neurodegenerative diseases: what makes it different from the other HDACs? *Mol. Neurodegener.* **8**, 7 (2013).
- Taes, I. *et al.* Hdac6 deletion delays disease progression in the SOD1G93A mouse model of ALS. *Hum. Mol. Genet.* **22**, 1783–1790 (2013).
- d'Ydewalle, C. *et al.* HDAC6 inhibitors reverse axonal loss in a mouse model of mutant HSPB1-induced Charcot-Marie-Tooth disease. *Nat. Med.* **17**, 968–974 (2011).
- Ackerley, S. *et al.* Neurofilament heavy chain side-arm phosphorylation regulates axonal transport of neurofilaments. *J. Cell Biol.* **161**, 489–495 (2003).

57. De Vos, K. J. *et al.* Familial amyotrophic lateral sclerosis-linked SOD1 mutants perturb fast axonal transport to reduce axonal mitochondria content. *Hum. Mol. Genet.* **16**, 2720–2728 (2007).
58. Morotz, G. M. *et al.* Amyotrophic lateral sclerosis-associated mutant VAPBP56S perturbs calcium homeostasis to disrupt axonal transport of mitochondria. *Hum. Mol. Genet.* **21**, 1979–1988 (2012).
59. De Vos, K. J. & Sheetz, M. P. Visualization and quantification of mitochondrial dynamics in living animal cells. *Methods Cell Biol.* **80**, 627–682 (2007).
60. De Vos, K. J., Allan, V. J., Grierson, A. J. & Sheetz, M. P. Mitochondrial function and actin regulate dynamin-related protein 1-dependent mitochondrial fission. *Curr. Biol.* **15**, 678–683 (2005).
61. Liu, Z. *et al.* A *Drosophila* model for LRRK2-linked parkinsonism. *Proc. Natl Acad. Sci. USA* **105**, 2693–2698 (2008).
62. Lin, C. H., Tsai, P. I., Wu, R. M. & Chien, C. T. LRRK2 G2019S mutation induces dendrite degeneration through mislocalization and phosphorylation of tau by recruiting autoactivated GSK3beta. *J. Neurosci.* **30**, 13138–13149 (2010).
63. Imai, Y. *et al.* Phosphorylation of 4E-BP by LRRK2 affects the maintenance of dopaminergic neurons in *Drosophila*. *EMBO J.* **27**, 2432–2443 (2008).
64. Lee, S. B., Kim, W., Lee, S. & Chung, J. Loss of LRRK2/PARK8 induces degeneration of dopaminergic neurons in *Drosophila*. *Biochem. Biophys. Res. Commun.* **358**, 534–539 (2007).
65. Dietzl, G. *et al.* A genome-wide transgenic RNAi library for conditional gene inactivation in *Drosophila*. *Nature* **448**, 151–156 (2007).
66. Greene, J. C. *et al.* Mitochondrial pathology and apoptotic muscle degeneration in *Drosophila* parkin mutants. *Proc. Natl Acad. Sci. USA* **100**, 4078–4083 (2003).
67. Kuznicki, M. L. & Gunawardena, S. *In vivo* visualization of synaptic vesicles within *Drosophila* larval segmental axons. *J. Vis. Exp.* **44**, 2151 doi:10.3791/2151 (2010).
68. Meulener, M. *et al.* *Drosophila* DJ-1 mutants are selectively sensitive to environmental toxins associated with Parkinson's disease. *Curr. Biol.* **15**, 1572–1577 (2005).

## Acknowledgements

We thank C. Chien, J. Chung, Y. Imai, W. Smith and C. Elliott for kind provision of the transgenic fly lines, M. Cookson (NIH, Bethesda, USA) for LRRK2 constructs, J. Gaertig

(University of Georgia, Athens GA) for the pSPORT6-MEC17 ( $\alpha$ TAT1) expression plasmid and T. Schwarz (Harvard Medical School) for technical advice. Stocks obtained from the Bloomington *Drosophila* Stock Center (NIH P40OD018537) were used in this study. This work was funded by grants from Parkinson's UK (G-0813 to K.J.D.V.), Wellcome Trust (078662 to C.C.J.M.) and MRC (MR/K005146/1 to K.J.D.V.; G0501573 to C.C.J.M.), a Wellcome/MRC Parkinson's Disease Consortium grant to UCL/IO/N, the University of Sheffield and the MRC Protein Phosphorylation Unit at the University of Dundee (WT089698) and an ERC Starting Grant (no. 309742 to A.J.W.). The Sheffield Light Microscopy Facility is supported by the Wellcome Trust (GR077544AIA) and a Wolfson Foundation Grant to SITraN funded the Leica SP5 confocal microscope.

## Author contributions

V.K.G., N.B.-H., R.M.S., G.S., A.M., M.O., A.J.W. and K.J.D.V. performed the experiments. C.C.J.M., A.J.W. and K.J.D.V. designed the experiments and directed the research. A.J.W. and K.J.D.V. wrote the manuscript.

## Additional information

**Supplementary Information** accompanies this paper at <http://www.nature.com/naturecommunications>

**Competing financial interests:** The authors declare no competing financial interests.

**Reprints and permission** information is available online at <http://npg.nature.com/reprintsandpermissions/>

**How to cite this article:** Godena, V. K. *et al.* Increasing microtubule acetylation rescues axonal transport and locomotor deficits caused by LRRK2 Roc-COR domain mutations. *Nat. Commun.* 5:5245 doi: 10.1038/ncomms6245 (2014).



This work is licensed under a Creative Commons Attribution 4.0 International License. The images or other third party material in this article are included in the article's Creative Commons license, unless indicated otherwise in the credit line; if the material is not included under the Creative Commons license, users will need to obtain permission from the license holder to reproduce the material. To view a copy of this license, visit <http://creativecommons.org/licenses/by/4.0/>